Perspectives and recent advances of two-dimensional III-nitrides: Material synthesis and emerging device applications

Article *in* Applied Physics Letters · April 2023

DOI: 10.1063/5.0145931

CITATIONS
5

READS
279

10 authors, including:

Yuanpeng Wu
University of Michigan
58 PUBLICATIONS **1,197** CITATIONS
SEE PROFILE

Ping Wang
139 PUBLICATIONS **1,864** CITATIONS
SEE PROFILE

Woncheol Lee
Seoul National University
25 PUBLICATIONS **444** CITATIONS
SEE PROFILE

Emmanouil Kioupakis
University of Michigan
169 PUBLICATIONS **5,634** CITATIONS
SEE PROFILE

Applied Physics Letters

RESEARCH ARTICLE | APRIL 17 2023

Perspectives and recent advances of two-dimensional III-nitrides: Material synthesis and emerging device applications

Yuanpeng Wu ; Ping Wang ; Woncheol Lee ; Anthony Aiello ; Parag Deotare ; Theodore Norris; Pallab Bhattacharya ; Mackillo Kira ; Emmanouil Kioupakis ; Zetian Mi

Appl. Phys. Lett. 122, 160501 (2023)
https://doi.org/10.1063/5.0145931

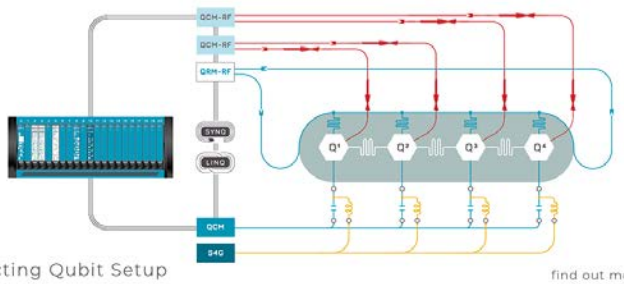

Applied Physics Letters PERSPECTIVE scitation.org/journal/apl

Perspectives and recent advances of two-dimensional III-nitrides: Material synthesis and emerging device applications

Cite as: Appl. Phys. Lett. **122**, 160501 (2023); doi: 10.1063/5.0145931
Submitted: 8 February 2023 · Accepted: 28 March 2023 ·
Published Online: 17 April 2023

Yuanpeng Wu,[1,a)] Ping Wang,[1] Woncheol Lee,[1] Anthony Aiello,[1] Parag Deotare,[1] Theodore Norris,[1] Pallab Bhattacharya,[1] Mackillo Kira,[1,a)] Emmanouil Kioupakis,[2,a)] and Zetian Mi[1,a)]

AFFILIATIONS

[1]Department of Electrical Engineering and Computer Science, University of Michigan, Ann Arbor, Michigan 48109, USA
[2]Department of Materials Science and Engineering, University of Michigan, Ann Arbor, Michigan 48109, USA

[a)]**Authors to whom correspondence should be addressed:** ypwu@umich.edu; mackkira@umich.edu; kioup@umich.edu; and ztmi@umich.edu

ABSTRACT

Both two-dimensional (2D) transitional metal dichalcogenides (TMDs) and III–V semiconductors have been considered as potential platforms for quantum technology. While 2D TMDs exhibit a large exciton binding energy, and their quantum properties can be tailored via heterostructure stacking, TMD technology is currently limited by the incompatibility with existing industrial processes. Conversely, III-nitrides have been widely used in light-emitting devices and power electronics but not leveraging excitonic quantum aspects. Recent demonstrations of 2D III-nitrides have introduced exciton binding energies rivaling TMDs, promising the possibility to achieve room-temperature quantum technologies also with III-nitrides. Here, we discuss recent advancements in the synthesis and characterizations of 2D III-nitrides with a focus on 2D free-standing structures and embedded ultrathin quantum wells. We overview the main obstacles in the material synthesis, vital solutions, and the exquisite optical properties of 2D III-nitrides that enable excitonic and quantum-light emitters.

I. INTRODUCTION

Two-dimensional (2D) semiconductors, such as transitional metal dichalcogenides (TMDs), exhibit unique electronic, optical, excitonic, and quantum properties and correlations[1–10] that have been probed with super-resolution,[11] exploited to create quantum phases in heterostructures,[12–14] flipped in few femtoseconds,[15] and resolved at attosecond resolution.[16] In particular, the Coulomb interaction (and exciton binding) is significantly enhanced in 2D TMDs[17] because the majority of Coulombic field lines propagate outside the 2D material. Unscreened exciton binding energy theoretically can reach up to 700 meV in MoS_2, as shown in Fig. 1.[18] However, it remains an open challenge that how to create practical TMD optoelectronic devices as long as TMD synthesis yields major disorder and low control and reproducibility of designed properties.[19,20]

With their great advantages in composition tunability,[21] high material quality,[22] and large-scale integrability,[23] III–V semiconductors have been exploited during the past decades in optoelectronics, including light-emitting diodes (LEDs),[24–27] lasers,[28–30] photodetectors,[31,32] solar cells, and artificial synthesis,[21,33] to name just a few. Additionally, III–V semiconductors have been explored as a potential candidate for excitonic devices[34,35] and quantum devices,[36] including single photon emitters,[37–39] quantum sensors,[40] and quantum-optical state control.[41–43] At the same time, III-arsenide-based devices are typically limited to operation at cryogenic temperatures due to the small exciton binding energies of less than 10 meV,[44–46] resulting from strong dielectric screening of the Coulomb interaction between electron and hole pairs as well as much lighter effective mass compared with GaN.[18,47]

Compared with III-arsenides, bulk wurtzite III-nitrides have a significantly larger exciton binding energies, ranging from 10 to 60 meV, as shown in Fig. 1.[19] Recent theoretical studies[48–52] have predicted that group III-nitride materials can adopt a stable graphite-like hexagonal crystal structure in their monolayer limit, exhibiting tunable energy bandgap from 2 to 9 eV. The recent theory also predicted that by exploiting the strong Coulomb interaction and excitons in monolayer III-nitrides, conventional low-efficiency AlGaN and indirect-bandgap hBN can be turned into high-brightness deep UV emitters,[53,54] which are the *only* alternative technology to replace

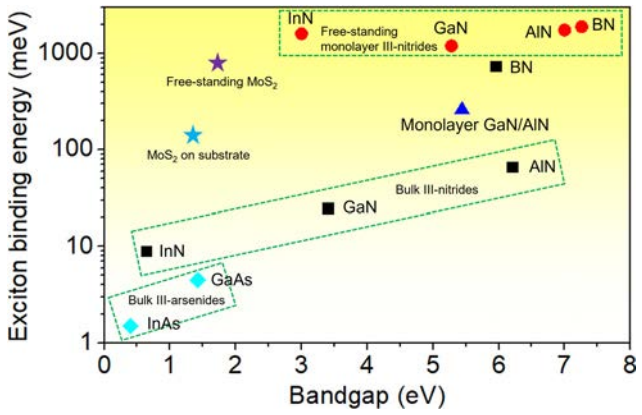

FIG. 1. Exciton binding energy of TMDs and monolayer III-nitrides plotted vs bandgap.

mercury lamps for water and air purification. To date, however, it has remained difficult to achieve 2D III-nitrides beyond small-scale domains. Consequently, many fundamental optical, electrical, excitonic, and quantum properties of 2D III-nitrides have remained unknown. Therefore, the design, discovery, and development of 2D III-nitride nanostructures with innovative electronic, optical, excitonic, and quantum properties will enable a broad spectrum of applications, from high-efficiency light absorbers[55] or light harvesting, deep UV light emitters for water/air purification, and room temperature single photon sources, to architectures for excitonic optoelectronics.

In this Perspective, we discuss the recent developments of next generation 2D III-nitride semiconductors, including monolayer InN, GaN, AlN, and hBN. The quantum theory and design, epitaxy, and characterization are presented. Their applications in achieving efficient light generation in the deep UV and room-temperature single photon emitters are also described. This Perspective provides a broad overview on the synthesis of 2D III-nitrides with desired properties for applications in next-generation optoelectronic, excitonic, and quantum devices.

II. SYNTHESIS OF 2D III-NITRIDES

To date, there is a significant gap between the theoretical prediction of 2D III-nitrides and the experimental realization of such structures. Although GaN-based 3D crystal structures have been extensively studied for LED lighting and power electronic applications, the epitaxy/synthesis of 2D III-nitrides is facing tremendous challenges. Depending on the preferred orbital hybridization configuration, III-nitrides can be divided into two categories. The sp^2 hybridized materials (such as hBN)[56,57] have mixed in-plane ionic/covalent bonding and primary van der Waals (vdW) interaction between layers along the [0001] direction. The weak vdW interlayer interaction enables the mechanical exfoliation of 2D hBN.[58] The sp^3 hybridized materials (such as InN, GaN, AlN, and their ternary and quaternary alloys) feature strong covalent/ionic bonding along all crystallographic directions,[59] making it almost impossible to mechanically exfoliate 2D nitrides from their bulk format. Moreover, it remains challenging to directly thin down GaN bulk to a few atomic layers by cleaving the tetrahedrally bonded surface along the (0001) plane.[60]

The hybridization configuration also affects the nucleation and crystal growth of III-nitrides during epitaxial growth. For example, the surface adatoms tend to be adsorbed and nucleate at the propagating edges of hBN, which leads to the formation of a layered 2D structure.[61] Wurtzite III-nitrides growth is essentially a 3D process with growth rate along different crystallographic directions determined by the surface energy anisotropies,[62] which makes it very difficult to realize only 2D growth in wurtzite III-nitrides. In addition, it is desired that the 2D structure can be separated from the epitaxial substrate and, therefore, can be transferred to arbitrary or functionalized substrates to facilitate subsequent device processing, which puts another demand on the material synthesis. Some of the major developments in the growth/synthesis 2D III-nitrides are briefly described as follows.

A. Monolayer III-nitrides

Monolayer III-nitrides are essentially quantum wells consisting of one atomic layer thin materials. By exploiting Coulomb engineering and excitons, Kioupakis *et al.* predicted that the radiative efficiency could be enhanced by up to three orders of magnitude due to the extreme quantum confinement, which reduces the polarization-induced separation of electrons and holes and enhances the Coulomb interaction.[54,55] Monolayer III-nitrides present an unexplored opportunity for realizing high-efficiency deep UV emission, which is critical for water/air purification and disinfection.[63] Experimentally, significantly enhanced Coulomb interaction can be achieved through quantum confinement between materials with large band offsets, wherein ultrawide bandgap Al(Ga)N materials are typically utilized as the barrier. The large band offsets ensure the confinement of charge carriers within the quantum wells.[64] Extensive efforts have been devoted to achieving embedded ultrathin (In)GaN in the epilayer structure.[65–69] However, interdiffusion of cations between the quantum well and barrier is often observed,[70,71] which makes the quantum confinement and the Coulomb enhancement effect elusive.

We have demonstrated the epitaxy of monolayer GaN embedded in AlN nanowires grown directly on Si substrate.[64,72] The epitaxy was performed under nitrogen-rich conditions. Figure 2(a) shows the scanning transmission electron microscopy (STEM) image of the as-grown heterostructure, wherein a monolayer of GaN in AlN matrix with relatively sharp interfaces can be identified. The significantly improved interface quality compared with ultrathin GaN/AlN grown in epilayer structure can be attributed to the nitrogen-rich growth condition utilized for N-polar nanostructures. During molecular beam epitaxy (MBE), a metal-rich growth regime is generally used to ensure a smooth surface; however, atomic steps tend to be formed in this growth regime, which causes discontinuity in monolayer GaN.[70] Under nitrogen-rich growth conditions, the growth front of the nanowires is free from excess metal adatoms, which can effectively prevent interfacial mixing due to variations in incorporation preferences of surface metal adatoms.

With interfacial quality significantly improved, the optical properties of ultrathin GaN can be readily tuned by varying the thickness/growth duration. As shown in Fig. 2(b), monolayer GaN embedded in AlN matrix exhibits strong emission at 240 nm, whereas two monolayer corresponds to 270 nm emission. Theoretical and experimental results also showed that the electronic and optical gap both increase with increasing the AlN barrier thickness [Fig. 2(c)]. The measured photon energies match well with the optical gap. The difference

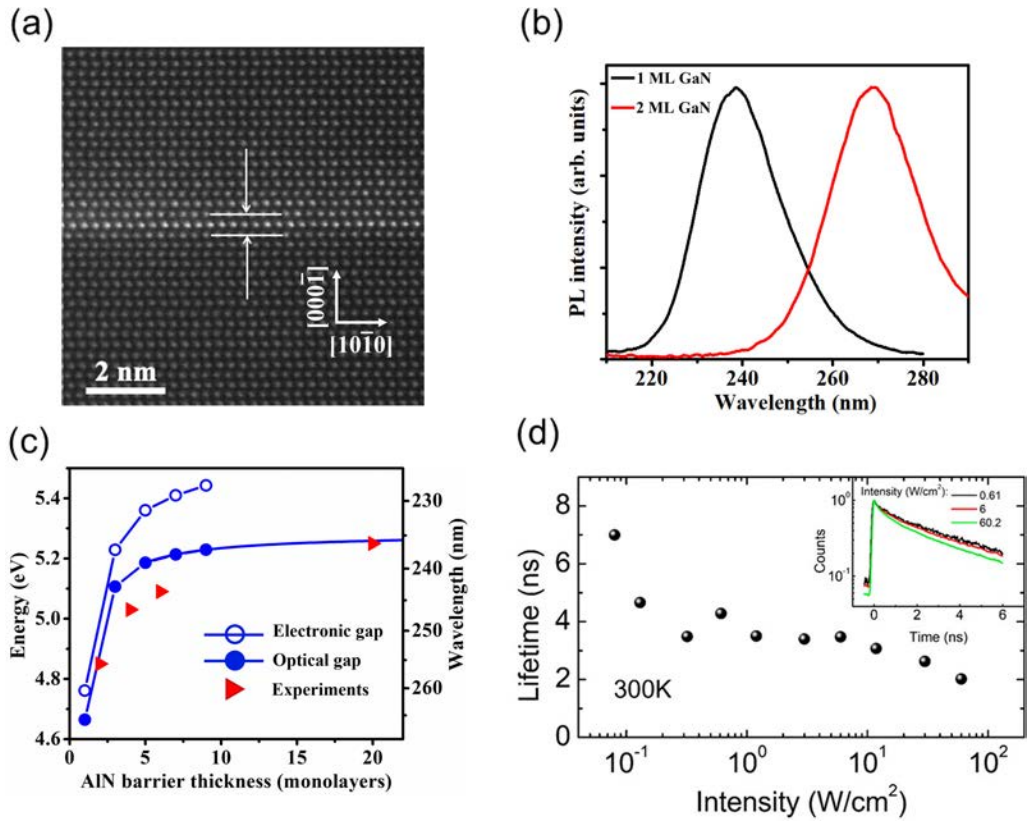

FIG. 2. (a) High-magnification STEM image of monolayer GaN embedded in AlN matrix. The epitaxial direction is along the [000$\bar{1}$] direction. (b) PL spectra of GaN/AlN heterostructure with monolayer and bilayer GaN. (c) Calculated electronic and optical gaps vs AlN barrier thickness. The red triangles are the experimentally measured peak energies. Lines connected to and extrapolated from the theory data points are guides to the eye. The exciton binding energies are indicated by the green arrow. (d) Recombination lifetime with excitation intensity at 300 K in monolayer GaN nanowire sample. The measured PL transients are shown in the inset of (d). Reproduced with permission from Wu *et al.*, Appl. Phys. Lett. **5**, 100350 (2020). Copyright 2022 AIP; and Aiello *et al.*, Nano Lett. **132**, 16587 (2019). Copyright 2022 ACS.

between the electronic and optical gap results in an exciton binding energy of 230 meV, which is well above the thermal energy at room temperature and is about one order of magnitude larger than that of bulk GaN. The enhanced exciton binding energy essentially results from enhanced Coulomb interactions of the electron–hole pairs confined in the ultrathin quantum well. Beyond an excitation power of 0.3 W/cm^2, the measured lifetime is relatively invariant with increasing excitation power [Fig. 2(d)], which agrees well with the features of exciton-related emission.[72]

B. Graphene encapsulation

In 2016, Balushi *et al.* reported the growth of 2D GaN using graphene encapsulation.[73] In this process, a graphene capping layer is used to stabilize the 2D GaN layer and promote Frank–van der Merwe growth. The 2D GaN layer is formed between graphene and the underlying SiC substrate, as shown in Fig. 3(a1). A direct energy bandgap of 5 eV was measured, in good agreement with theory. The obtained 2D GaN has an R3m space group and covalently bonds with the epitaxial substrate as shown in Fig. 3(a2), making it almost impossible to separate the 2D GaN from the substrate. Such a method has also been used to realize 2D InN and 2D AlN recently.[74,75] In these studies, the formation of 2D III-nitride layers was made possible by Ga (or Al) adatom intercalation through defects in the graphene layer. Consequently, the growth of 2D III-nitride layers is extremely sensitive to the defect distribution in graphene. In addition, this growth process results in the extensive formation of 3D III-nitrides on graphene, leading to a mixture of 3D and 2D structures. It is difficult to achieve uniform 2D III-nitrides beyond small-scale domains. To date, there have been no experimental studies of photoluminescence emission, charge carrier transport, and excitonic properties.

C. Surface-confined, metal-assisted growth

In 2018, Chen *et al.* showed that free-standing 2D wurtzite GaN can be synthesized on liquid gallium via a surface-confined nitridation reaction in a chemical vapor deposition chamber.[76] In this process, the liquid gallium droplet is spread on a tungsten (W) foil, and urea is supplied as a precursor for the nitrogen source. The ultrathin GaN is also reflected by the low-magnification transmission electron microscopy (TEM) image, as shown in Fig. 3(b1). The wurtzite crystal structure is confirmed by the high-magnification TEM images, as shown in

Figs. 3(b2) and 3(b3). The successful synthesis of 2D GaN was attributed to the stratified Ga/Ga-W structure, wherein an ultrathin liquid Ga layer exists at the growth front and participates in the growth of 2D GaN with micrometer size. At the growth temperature of 1080 °C, the Ga-W under the surficial Ga layer remains in a solid state and prevents thickening of the as-grown 2D GaN as excess N adatoms at the surface are deprived by the W atom due to its stronger nitridation ability. The obtained 2D GaN shows uniform lattice parameters and superior optical quality, including blue-shifted photoluminescence and enhanced internal quantum efficiency. More importantly, the 2D GaN can be transferred onto an SOI substrate, and a field effect transistor based on the 2D GaN was demonstrated. It is worth noting that 2D

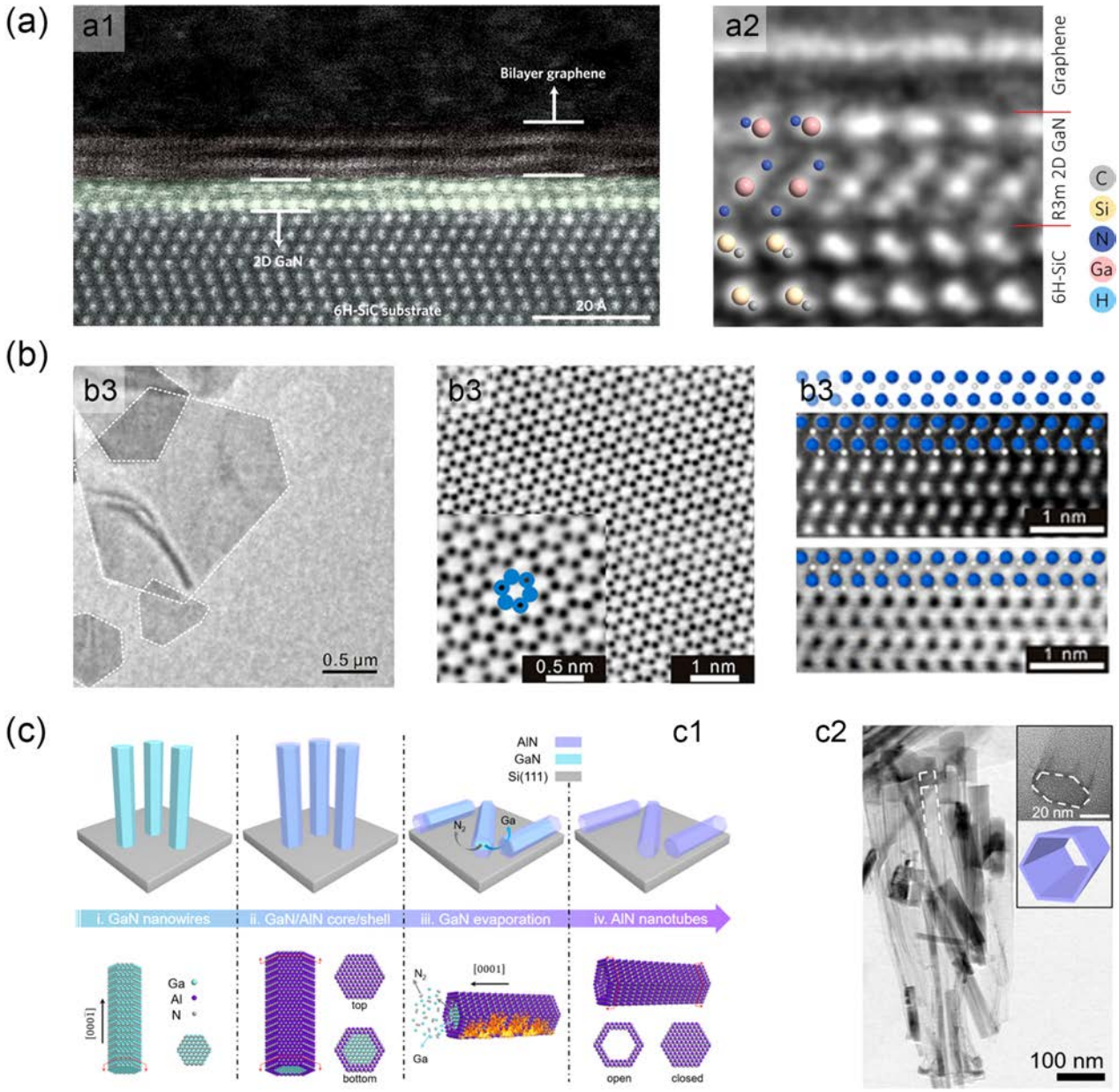

FIG. 3. (a) 2D GaN synthesized using the graphene encapsulation method: cross-sectional HAADF-STEM image (a1) and ABF-STEM image (a2) of 2D GaN. (b) 2D GaN synthesized via the surface-confined and metal-assisted growth method: low-magnification TEM image (b1), BF STEM image acquired along [0001] zone axis (b2), and HAADF (top panel) and BF STEM (bottom panel) images acquired along [$10\bar{1}0$] zone axis (b3) for 2D GaN crystals. (c) Atomically thin AlN synthesized through selective thermal evaporation: schematics and atomic models of the fabrication process (c1) and low-magnification TEM image of atomically thin AlN nanotubes (c2). Reproduced with permission from Balushi *et al.*, Nat. Mater. **15**, 1166–1171 (2016). Copyright 2022 Springer Nature; Chen *et al.*, J. Am. Chem. Soc. **140**, 16392 (2018). Copyright 2022 ACS; and Wang *et al.*, Adv. Funct. Mater. **29**, 1902608 (2019). Copyright 2022 Wiley.

III-nitrides have much larger bandgap compared with 2D TMDs, and the large bandgap can potentially enable high on/off ratio in switching devices and is ideally suited for deep UV optoelectronics. Based on this synthesis method, ammonolysis of liquid Ga was also reported to obtain 2D GaN with a thickness of 1.3 nm.[77]

D. Selective thermal evaporation

In 2019, Wang *et al.* reported the fabrication of atomically thin AlN by combining epitaxial casting with selective thermal evaporation.[78] The first step of this synthesis process is epitaxial casting. GaN/AlN core/shell nanowires were vertically grown on a Si substrate using a plasma-assisted molecular beam epitaxy (MBE) system. The thickness of AlN shell was controlled by the growth duration. The second step is selective thermal evaporation. The as-grown GaN/AlN core/shell nanowires ensemble was dispersed on a hydrophilic Si substrate (or other high-temperature resistant hydrophilic substrate, such as sapphire or SiC), then loaded into an ultrahigh vacuum MBE chamber, and performed a thermal evaporation at a temperature higher than the GaN decomposition temperature but lower than the AlN decomposition temperature, as schematically shown in Fig. 3(c1). Due to the large difference in the decomposition activation energy for GaN and AlN, the GaN core nanowire was decomposed into Ga and N and further evaporated from the bottom open end. Therefore, only the robust AlN shell survived after the high-temperature thermal treatment, forming atomically thin AlN nanotubes as confirmed by the high-magnification TEM images [Fig. 3(c2)]. The bandgap of such quasi-2D AlN was characterized by using x-ray photoelectron spectroscopy and spatially resolved electron energy loss spectroscopy measurements, showing an extremely large bandgap of 9.2 ± 0.1 eV for the AlN nanotubes with a wall thickness of two monolayers.[78] This bandgap value is consistent with the bandgap reported for the 2D AlN grown using the graphene encapsulation method.[74]

E. Ultrahigh temperature molecular beam epitaxy of monolayer hBN

Interestingly, hBN is both a structurally compatible material with Al(Ga)N and an ideal substrate for the emerging 2D TMD materials.[58,79] Previous studies of hBN have been largely focused on the use of mechanical exfoliation[80] or chemical vapor deposition,[81,82] which suffers from poor interface properties, high concentrations of unintentional impurity incorporation, and large densities of defects. As an opportunity for improving hBN quality, MBE offers ultimate control down to the atomic scale. However, the conventional MBE growth of BN has been limited by the lack of suitable techniques to evaporate boron source material (melting temperature 2076 °C), and the relatively low substrate heater temperature capabilities (often limited to below 1000 °C) to achieve enhanced surface migration of B atoms. We have recently implemented an unconventional MBE system, which is equipped with an ultrahigh temperature heater (up to 1800 °C) and a retrofitted multi-pocket e-beam source to provide stable thermal evaporation of ultrahigh purity elemental boron. We have demonstrated an hBN/AlN based light-emitting diode (LED), which can operate efficiently at 210 nm.[83]

While 2D wurtzite III-nitrides and hBN have been demonstrated using various synthesis methods, there has been a growing interest to control over the nucleation and crystallinity of the 2D nitrides for functional device application. The lack of controllability originates from the complex nucleation environment, wherein the epitaxial substrate surface consists of atomic steps with different heights, crystalline edges with different interfacial energies, and polycrystalline domains with various orientations, which prevent a precise control of the synthesis of 2D nitrides. Recently, we have developed a scalable and controllable synthesis of monolayer 2D hBN on graphene by controlling the initial nucleation process.[84] As schematically shown in Fig. 4(a), the surface of graphene substrate has two kinds of interfaces, namely, zigzag (ZZ) atomic edges and armchair (AC) edges. In an uncontrolled epitaxy, hBN nucleates on both interfaces, causes random interfaces, and prevents obtaining large-scale unidirectional hBN with single crystallinity. For controlled synthesis, the nucleation at the ZZ atomic edges of graphene is significantly suppressed. This is achieved by performing epitaxy at an ultrahigh temperature (1600 °C), wherein only nucleation at energetically stable interfaces exists. Subsequently, hBN exclusively grows at AC atomic edges, which results in uniform, faultless, and wafer scale epitaxy of 2D hBN, as shown in Fig. 4(b). The controlled synthesis of monolayer 2D hBN offers a promising opportunity to explore the indirect-to-direct bandgap crossover in hBN.[85]

Figure 4(c) shows the spectra collected from the monolayer hBN/HOPG sample measured at 12 K. The 5.86 eV peak is assigned to the multilayer hBN. The 6.12 eV peak matches well with the dip in the reflection spectrum measured at 300 K and can be assigned to the monolayer emission from hBN. Our first-principles calculations based on the density functional theory and the many-body perturbation theory results showed that free-standing monolayer hBN has a predicted bandgap of 8 eV. We found that the graphene layer adjacent to the hBN layer can cause giant bandgap renormalization of up to 1 eV, attributed to the metallic nature of graphene. This metallic nature can cause extreme screening of Coulomb interaction of charge carriers within hBN. For free-standing monolayer hBN, the calculated exciton binding energy can reach 2.3 eV, as shown in Fig. 4(d). With three monolayers of graphene present, the exciton binding energy of hBN reduces to 0.7 eV due to the strong metallic screening by graphene. The three monolayers of graphene are sufficient to converge the exciton binding energy, which is very close to the value for the semi-infinite HOPG substrate. The wavefunction was observed to be confined within the monolayer hBN, which further confirms the 2D exciton nature and strong light–matter interactions associated with measured photoluminescence emission.

III. EMERGING APPLICATIONS OF 2D III-NITRIDES

Unlike TMD, III-nitride nanoscale materials can be grown by industry standard epitaxial techniques and are compatible with traditional semiconductor processing, thus enabling scalability for real-world applications. Conventional AlGaN exhibits poor deep UV emission, due to the large densities of defects, polarization fields, and transverse magnetic (TM) polarized emission. It was predicted that monolayer GaN can exhibit transverse electric (TE) polarized emission, which enables efficient extraction of deep UV light emission.[54] UV light sources have been reported by using ultrathin GaN quantum structures as the active regions.[64,68,69,71] Figure 5(a) is a schematic of the AlN *p-i-n* structure with three periods of monolayer GaN incorporated.[64] The devices show deep UV-C electroluminescence (EL) with

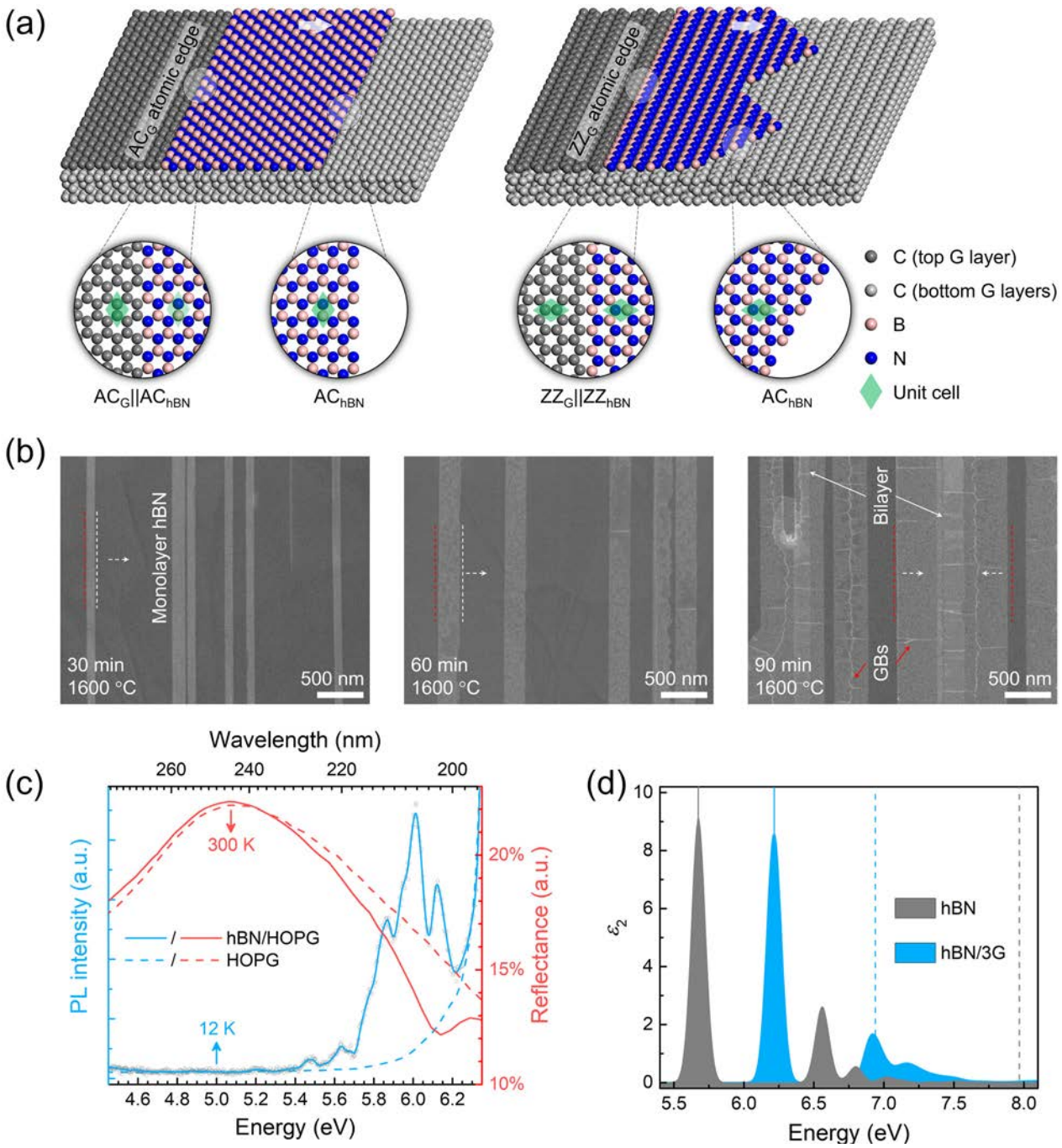

FIG. 4. (a) Schematics of monolayer hBN grown along the armchair (ACG) (left) and zigzag (ZZG) (right) graphene atomic edges, forming straight and jagged nanoribbons, respectively. All growth fronts of monolayer hBN are terminated with AC hBN edges. The magnifications show the atomic configurations of the ACG||AC hBN and ZZG||ZZ hBN in-plane interfaces, and the AC hBN growth fronts. The white arrows point to the growth direction. (b) Evolution of straight monolayer hBN nanoribbons is followed after 30, 60, and 90 min growth time at 1600 °C. (c) Measured, time-integrated PL spectra (blue curves, 12 K) and reflectance spectra (red curves, 300 K) of monolayer hBN/HOPG heterostructure (solid curves) and HOPG substrate (dashed curves). The gray circles are the PL data for monolayer hBN/HOPG heterostructures, while the blue solid curve is the corresponding smoothed curve. (d) Calculated absorption spectrum of a free-standing monolayer hBN (gray area) and monolayer hBN on three graphene layers (blue area). The vertical dashed lines indicate the quasiparticle bandgap, and the vertical solid lines show the 1s-exciton state position. Reproduced with permission from Wang *et al.*, Adv. Mater. **5**, 72 (2022). Copyright 2022 Wiley.

peak wavelength ~240 nm. Current-dependent EL measurements show that the device features an ultra-stable emission with negligible peak wavelength shift. The integrated EL intensity increases linearly with increasing injection current without apparent efficiency droop up to 40 A/cm^2, as shown in Fig. 5(b). It is worth noting that in conventional AlGaN quantum well-based UV LEDs, the efficiency droop happens when the current density is below 10 A/cm^2.[86] The suppression of efficiency droop could be attributed to the efficient excitonic radiative recombination. The monolayer III-nitrides support not only excitons but also biexcitons and dropletons.[41] Such quasiparticles dominate quantum material properties from exciton interactions to emission and detection of entangled photons.

Figure 5(c) shows that monolayer In(Ga)N embedded in GaN nanowires can be used to achieve single photon emission.[87] In this work, the nanowires array is fabricated by nanoimprinting lithography and dry/wet etching, followed by capping of additional GaN

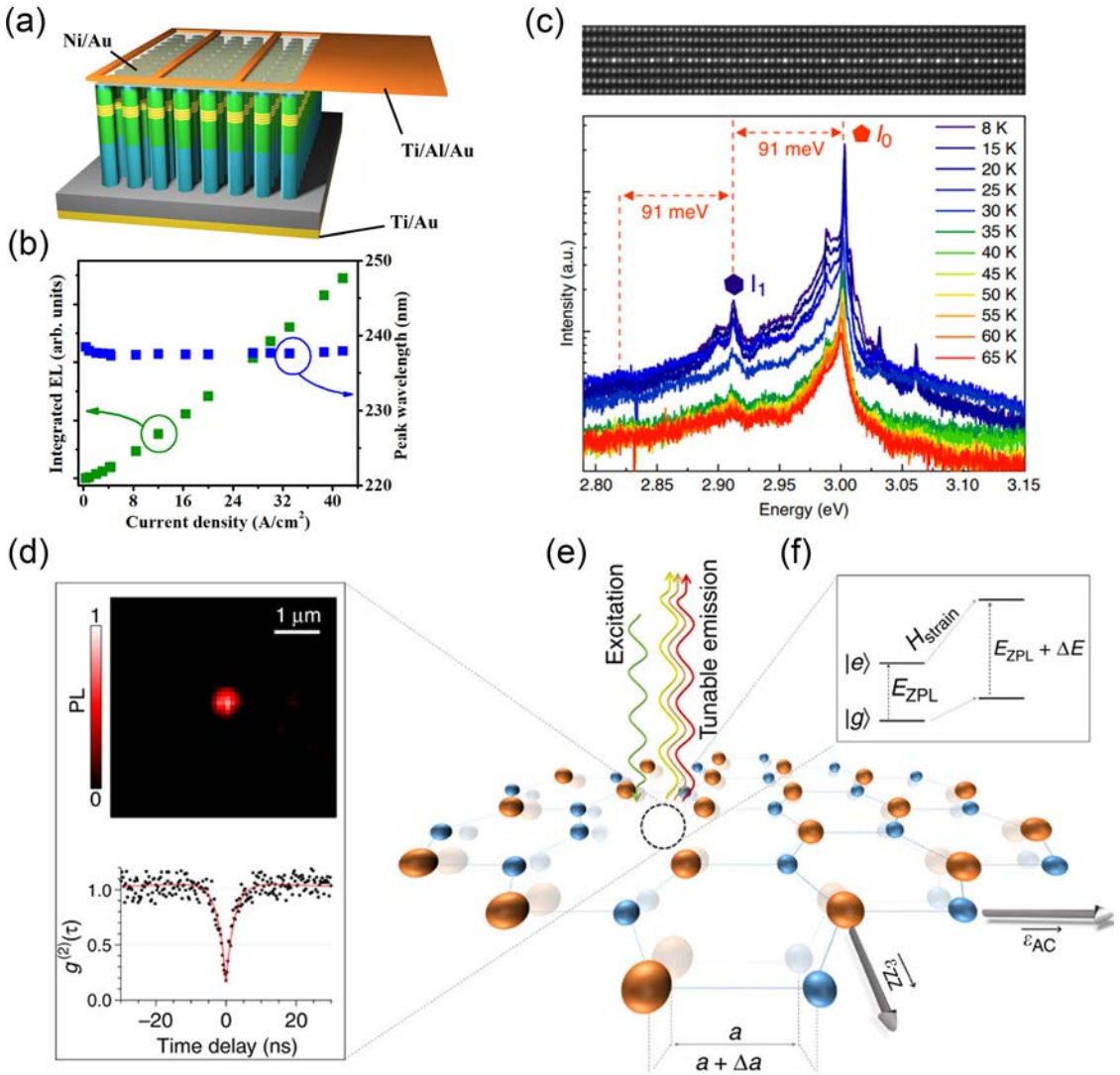

FIG. 5. (a) Schematic illustration of the fabricated large area monolayer GaN deep UV LED. (b) Variations of the integrated electroluminescence intensity (green) and peak position (blue) vs injection current. The measured device size is 300 × 300 μm^2. (c) High resolution TEM image of the monolayer In(Ga)N/GaN heterostructure and corresponding temperature-dependent PL spectra on the log scale. (d) Top image shows the normalized intensity of emission for an isolated single photon emitter in layered hBN when excited non-resonantly. The graph in the bottom is the second-correlation histogram of the quantum emission from the atom-like defect showing clear antibunching at zero time delay [$g^2(0) < 0.5$]. (e) Schematic representation of the hBN crystal lattice composed of regular hexagons with alternated atoms of N (blue) and B (orange). The dotted black circle shows an atom-like defect with an N atom missing and an adjacent B atom substituted by an N. Tensile strain along the armchair (AC) and zigzag (ZZ) directions produces a deformation of the crystal with a change Δa of N–B bond length. Strain results in a shift of the energy levels of the atom-like defect and allows one to tune the emission energy. (f) Drawing of a simplified energy level diagram showing the effect of strain. The emission energy can be strain-tuned of ΔE from the initial zero phonon line energy. Reproduced with permission from Grosso *et al.*, Nat. Commun. 5, 72 (2017). Copyright 2022 NPG.

conformal shell to reduce the nonradiative recombination. The series of peaks shown in the PL spectra have a typical linewidth of 900 μeV. The dominant peak features an asymmetric broadening on the low-energy side. The excitonic emission peak remains sharp until 30 K, which is significantly higher than the decoherence temperature reported in III-arsenide-based single photon emitters. The broadening of the PL spectrum with temperature can be attributed to the increased acoustic phonon-related broadening, which results in a slight redshift in the peak energies. Phonon side bands related to LO phonons are also observed, and the energy separation of 91 meV agrees well with the reported LO phonon energy in GaN. The identification of single photon emission was performed via Hanbury-Brown and Twiss (HBT) setup at 8 K. The obtained $g^2(0)$ value is 0.28 ± 0.09, which indicates the nature of the isolation of the transition between quantum states.

Crystallographic antisite defect in 2D hBN, namely, N_BV_N, features atomic-like structure and can be exploited to achieve single photon emission at room temperature.[88] The second-order correlation function $g^2(0)$ shows the anti-bunched photon characteristics measured from PL measurements at room temperature, mostly from the atom-like defect. In this work, single photon purity $g^2(0)$ of 0.077 was obtained, as shown in Fig. 5(d). Moreover, due to the ultrahigh stretchability of 2D structure, the emission spectra can be readily tuned by applying external strain along AC and ZZ directions of hBN, as schematically shown in Fig. 5(e), which modifies the electronic energy levels of hBN. Subsequently, the zero phonon line E_{ZPL} shows a shift of ΔE, and the emission peak can be tuned up to 6 meV experimentally as shown in Fig. 5(f).

IV. CONCLUSION

We have shown that III-nitrides in their 2D form have exquisite properties that could be beneficial for emerging applications in deep UV optoelectronics, optoexcitonics, and quantum technologies. Embedded ultrathin III-nitrides have excellent controllability in material synthesis, especially when selective area epitaxy is utilized. Plenty of areas related to embedded ultrathin III-nitrides remain to be explored. For example, by utilizing the coupling between two ultrathin quantum wells separated by an ultrathin barrier, we can achieve spatially indirect excitons (IXs). Such IXs exhibit extended radiative lifetime and, therefore, pave the way toward excitonic devices. So far, most of the optical and electrical measurements are performed on an ensemble of an arrayed nanostructure or a broad area of planar devices, which can maximize the signals but unavoidably includes the contributions from structures with varied strain distribution, thickness, and alloy compositional inhomogeneity. Quantum applications require both controlling and detecting quantum properties exclusively from single monolayer III-nitride structures. The embedded ultrathin III-nitrides are compatible with existing p/n-type doping that is paramount for device applications. Currently, 2D free-standing III-nitride synthesis is under rapid development and is particularly attractive due to the extremely large exciton binding energy (above 1 eV) because of reduced dielectric screening. There are still challenges in defect control, efficient transfer of 2D free-standing III-nitrides, and achieving electrically driven devices for practical optoelectronic and quantum device applications. Precise experimental control of 2D materials quantum excitations could be realized with a combination of strong lightwave[11,15,16,89] or refined quantum-spectroscopic excitations.[41,42,90] It is worth noting that ferroelectric III-nitrides, such as ScAlN and ScGaN,[91,92] have also been demonstrated recently. With the above-mentioned methods of synthesizing 2D structures, there exist promising opportunities for the exploration of 2D ferroelectric III-nitrides with significantly enhanced nonlinear optical and quantum properties.

ACKNOWLEDGMENTS

This work was supported by the Army Research Office (ARO) (Nos. W911NF-17–1-0312 and W911NF1810299), the National Science Foundation (NSF) (Nos. DMR-1807984 and 2118809), the Blue Sky Program in the College of Engineering at the University of Michigan, and the W. M. Keck Foundation.

AUTHOR DECLARATIONS

Conflict of Interest

Some IP related to this work has been licensed to NS Nanotech, Inc., which was co-founded by Z. Mi. The University of Michigan and Mi have a financial interest in the company.

Author Contributions

Yuanpeng Wu: Conceptualization (equal); Data curation (equal); Formal analysis (equal); Investigation (equal); Methodology (equal); Validation (equal); Writing – original draft (lead); Writing – review & editing (equal). **Zetian Mi:** Conceptualization (equal); Data curation (equal); Formal analysis (equal); Funding acquisition (equal); Investigation (equal); Methodology (equal); Project administration (equal); Resources (equal); Supervision (equal); Validation (equal); Writing – review & editing (equal). **Ping Wang:** Conceptualization (supporting); Data curation (supporting); Formal analysis (supporting); Investigation (supporting); Methodology (supporting); Validation (supporting); Writing – original draft (supporting); Writing – review & editing (supporting). **Woncheol Lee:** Formal analysis (supporting); Investigation (supporting); Methodology (supporting); Validation (supporting); Writing – review & editing (supporting). **Anthony Aiello:** Formal analysis (supporting); Investigation (supporting); Methodology (supporting). **Parag B. Deotare:** Conceptualization (supporting); Formal analysis (supporting); Funding acquisition (supporting); Investigation (supporting); Methodology (supporting); Resources (supporting); Validation (supporting). **Theodore B. Norris:** Conceptualization (supporting); Formal analysis (supporting); Funding acquisition (supporting); Investigation (supporting); Methodology (supporting); Resources (supporting); Validation (supporting). **Pallab K. Bhattacharya:** Conceptualization (supporting); Formal analysis (supporting); Funding acquisition (supporting); Investigation (supporting); Methodology (supporting); Resources (supporting); Validation (supporting); Writing – review & editing (supporting). **Mackillo Kira:** Conceptualization (equal); Formal analysis (equal); Funding acquisition (equal); Investigation (equal); Methodology (equal); Resources (equal); Validation (equal); Writing – review & editing (equal). **Emmanouil Kioupakis:** Conceptualization (equal); Formal analysis (equal); Funding acquisition (equal); Investigation (equal); Methodology (equal); Project administration (equal); Resources (equal); Validation (equal); Writing – review & editing (equal).

DATA AVAILABILITY

The data that support the findings of this study are available from the corresponding authors upon reasonable request.

REFERENCES

[1]A. K. Geim and I. V. Grigorieva, Nature **499**, 419–425 (2013).
[2]J. S. Ross, P. Klement, A. M. Jones, N. J. Ghimire, J. Yan, D. G. Mandrus, T. Taniguchi, K. Watanabe, K. Kitamura, W. Yao, D. H. Cobden, and X. Xu, Nat. Nanotechnol. **9**, 268–272 (2014).
[3]S. Wu, S. Buckley, J. R. Schaibley, L. Feng, J. Yan, D. G. Mandrus, F. Hatami, W. Yao, J. Vuckovic, A. Majumdar, and X. Xu, Nature **520**, 69–72 (2015).
[4]M. Bernardi, M. Palummo, and J. C. Grossman, Nano Lett. **13**, 3664–3670 (2013).
[5]O. Lopez-Sanchez, D. Lembke, M. Kayci, A. Radenovic, and A. Kis, Nat. Nanotechnol. **8**, 497–501 (2013).
[6]O. Salehzadeh, M. Djavid, N. Hong Tran, I. Shih, and Z.n Mi, "Optically Pumped Two-Dimensional MoS_2 Lasers Operating at Room-Temperature," Nano Letters. **15**(8), 5302–5306 (2015).
[7]D. Xiao, G.-B. Liu, W. Feng, X. Xu, and W. Yao, Phys. Rev. Lett. **108**, 196802 (2012).
[8]K. S. Novoselov, A. Mishchenko, A. Carvalho, and A. H. Castro Neto, Science **353**, aac9439 (2016).
[9]X. Duan, C. Wang, J. C. Shaw, R. Cheng, Y. Chen, H. Li, X. Wu, Y. Tang, Q. Zhang, A. Pan, J. Jiang, R. Yu, Y. Huang, and X. Duan, Nat. Nanotechnol. **9**, 1024–1030 (2014).
[10]K. F. Mak, C. Lee, J. Hone, J. Shan, and T. F. Heinz, Phys. Rev. Lett. **105**, 136805 (2010).
[11]M. Borsch, C. P. Schmid, L. Weigl, S. Schlauderer, N. Hofmann, C. Lange, J. T. Steiner, S. W. Koch, R. Huber, and M. Kira, Science **370**, 1204–1207 (2020).
[12]Y. Zhou, J. Sung, E. Brutschea, I. Esterlis, Y. Wang, G. Scuri, R. J. Gelly, H. Heo, T. Taniguchi, K. Watanabe, G. Zarand, M. D. Lukin, P. Kim, E. Demler, and H. Park, Nature **595**, 48–52 (2021).
[13]Y. Xu, S. Liu, D. A. Rhodes, K. Watanabe, T. Taniguchi, J. Hone, V. Elser, K. F. Mak, and J. Shan, Nature **587**, 214–218 (2020).
[14]Y. Cao, V. Fatemi, S. Fang, K. Watanabe, T. Taniguchi, E. Kaxiras, and P. Jarillo-Herrero, Nature **556**, 43–50 (2018).
[15]J. Freudenstein, M. Borsch, M. Meierhofer, D. Afanasiev, C. P. Schmid, F. Sandner, M. Liebich, A. Girnghuber, M. Knorr, M. Kira, and R. Huber, Nature **610**, 290–295 (2022).
[16]F. Langer, C. P. Schmid, S. Schlauderer, M. Gmitra, J. Fabian, P. Nagler, C. Schuller, T. Korn, P. G. Hawkins, J. T. Steiner, U. Huttner, S. W. Koch, M. Kira, and R. Huber, Nature **557**, 76–80 (2018).
[17]B. Zhu, X. Chen, and X. Cui, Sci. Rep. **5**, 9218 (2015).
[18]A. Chernikov, T. C. Berkelbach, H. M. Hill, A. Rigosi, Y. Li, O. B. Aslan, D. R. Reichman, M. S. Hybertsen, and T. F. Heinz, Phys. Rev. Lett. **113**, 076802 (2014).
[19]Y. Wu, X. Liu, A. Pandey, P. Zhou, W. J. Dong, P. Wang, J. Min, P. Deotare, M. Kira, E. Kioupakis, and Z. Mi, Prog. Quantum Electron. **85**, 100401 (2022).
[20]T. L. Purz, E. W. Martin, W. G. Holtzmann, P. Rivera, A. Alfrey, K. M. Bates, H. Deng, X. Xu, and S. T. Cundiff, J. Chem. Phys. **156**, 214704 (2022).
[21]Y. Wang, Y. Wu, K. Sun, and Z. Mi, Mater. Horiz. **6**, 1454–1462 (2019).
[22]Y. Sun, W. Shin, D. A. Laleyan, P. Wang, A. Pandey, X. Liu, Y. Wu, M. Soltani, and Z. Mi, Opt. Lett. **44**, 5679–5682 (2019).
[23]G. Tang, M. H. Kwan, R. Y. Su, F. W. Yao, Y. M. Lin, J. L. Yu, T. Yang, C.-H. Chern, T. Tsai, H. C. Tuan, A. Kalnitsky, and K. J. Chen, IEEE Electron Device Lett. **39**, 1362–1365 (2018).
[24]Y. Zhao, J. Liang, Q. Zeng, Y. Li, P. Li, K. Fan, W. Sun, J. Lv, Y. Qin, Q. Wang, J. Tao, and W. Wang, Opt. Express **29**, 20217–20228 (2021).
[25]X. Liu, Y. Sun, Y. Malhotra, A. Pandey, P. Wang, Y. Wu, K. Sun, and Z. Mi, Photonics Res. **10**, 587 (2022).
[26]X. Liu, Y. Wu, Y. Malhotra, Y. Sun, Y. H. Ra, R. Wang, M. Stevenson, S. Coe-Sullivan, and Z. Mi, J. Soc. Inf. Disp. **28**, 410–417 (2020).
[27]Y. Wu, Y. Xiao, I. Navid, K. Sun, Y. Malhotra, P. Wang, D. Wang, Y. Xu, A. Pandey, M. Reddeppa, W. Shin, J. Liu, J. Min, and Z. Mi, Light: Sci. Appl. **11**, 294 (2022).
[28]S. Zhao, X. Liu, Y. Wu, and Z. Mi, Appl. Phys. Lett. **109**, 191106 (2016).
[29]N. V. Kryzhanovskaya, A. I. Likhachev, S. A. Blokhin, A. A. Blokhin, E. V. Pirogov, M. S. Sobolev, A. V. Babichev, A. G. Gladyshev, L. Y. Karachinsky, I. I. Novikov, V. V. Andryushkin, D. V. Denisov, and A. Y. Egorov, Laser Phys. Lett. **19**, 075801 (2022).
[30]M. Shan, Y. Zhang, M. Tian, R. Lin, J. A. Jiang, Z. Zheng, Y. Zhao, Y. Lu, Z. Feng, W. Guo, J. Dai, C. Chen, F. Wu, and X. Li, ACS Photonics **8**, 1264–1270 (2021).
[31]A. Aiello, Y. Wu, Z. Mi, and P. Bhattacharya, Appl. Phys. Lett. **116**, 061104 (2020).
[32]D. Wang, X. Liu, Y. Kang, X. Wang, Y. Wu, S. Fang, H. Yu, M. H. Memon, H. Zhang, W. Hu, Z. Mi, L. Fu, H. Sun, and S. Long, Nat. Electron. **4**, 645–652 (2021).
[33]Y. Wang, Y. Wu, J. Schwartz, S. H. Sung, R. Hovden, and Z. Mi, Joule **3**, 2444–2456 (2019).
[34]J. Ben, X. Liu, C. Wang, Y. Zhang, Z. Shi, Y. Jia, S. Zhang, H. Zhang, W. Yu, D. Li, and X. Sun, Adv. Mater. **33**, e2006761 (2021).
[35]D. Ma, X. Rong, X. Zheng, W. Wang, P. Wang, T. Schulz, M. Albrecht, S. Metzner, M. Muller, O. August, F. Bertram, J. Christen, P. Jin, M. Li, J. Zhang, X. Yang, F. Xu, Z. Qin, W. Ge, B. Shen, and X. Wang, Sci. Rep. **7**, 46420 (2017).
[36]C. Fournier, A. Plaud, S. Roux, A. Pierret, M. Rosticher, K. Watanabe, T. Taniguchi, S. Buil, X. Quelin, J. Barjon, J. P. Hermier, and A. Delteil, Nat. Commun. **12**, 3779 (2021).
[37]T. Miyazawa, K. Takemoto, Y. Nambu, S. Miki, T. Yamashita, H. Terai, M. Fujiwara, M. Sasaki, Y. Sakuma, M. Takatsu, T. Yamamoto, and Y. Arakawa, Appl. Phys. Lett. **109**, 132106 (2016).
[38]F. Liu, X. Rong, Y. Yu, T. Wang, B. W. Sheng, J. Q. Wei, S. F. Liu, J. J. Yang, F. Bertram, F. J. Xu, X. L. Yang, Z. H. Zhang, Z. X. Qin, Y. T. Zhang, B. Shen, and X. Q. Wang, Appl. Phys. Lett. **116**, 142104 (2020).
[39]C. Lyu, F. Liu, Z. Zang, T. Wang, Y. Li, X. Xu, X. Wang, and Y. Ye, AIP Adv. **11**, 115101 (2021).
[40]J. Lahnemann, A. Ajay, M. I. Den Hertog, and E. Monroy, Nano Lett. **17**, 6954–6960 (2017).
[41]A. E. Almand-Hunter, H. Li, S. T. Cundiff, M. Mootz, M. Kira, and S. W. Koch, Nature **506**, 471–475 (2014).
[42]M. Kira and S. W. Koch, Phys. Rev. A **73**, 013813 (2006).
[43]M. Kira and S. W. Koch, *Semiconductor Quantum Optics* (Cambridge University Press, 2012).
[44]S. Tamariz, G. Callsen, and N. Grandjean, Appl. Phys. Lett. **114**, 082101 (2019).
[45]M. Baranowski, P. Plochocka, R. Su, L. Legrand, T. Barisien, F. Bernardot, Q. Xiong, C. Testelin, and M. Chamarro, Photonics Res. **8**, A50 (2020).
[46]S. B. Nam, D. C. Reynolds, C. W. Litton, R. J. Almassy, T. C. Collins, and C. M. Wolfe, Phys. Rev. B **13**, 761–767 (1976).
[47]K. S. Thygesen, 2D Mater. **4**, 022004 (2017).
[48]A. V. Kolobov, P. Fons, J. Tominaga, B. Hyot, and B. Andre, Nano Lett. **16**, 4849–4856 (2016).
[49]D. Kecik, A. Onen, M. Konuk, E. Gurbuz, F. Ersan, S. Cahangirov, E. Akturk, E. Durgun, and S. Ciraci, Appl. Phys. Rev. **5**, 011105 (2018).
[50]M. C. Lucking, W. Xie, D. H. Choe, D. West, T. M. Lu, and S. B. Zhang, Phys. Rev. Lett. **120**, 086101 (2018).
[51]A. Onen, D. Kecik, E. Durgun, and S. Ciraci, Nanoscale **10**, 21842–21850 (2018).
[52]A. V. Kolobov, P. Fons, Y. Saito, J. Tominaga, B. Hyot, and B. André, Phys. Rev. Mater. **1**, 024003 (2017).
[53]A. Aiello, Y. Wu, A. Pandey, P. Wang, W. Lee, D. Bayerl, N. Sanders, Z. Deng, J. Gim, and K. Sun, Nano Lett. **19**, 7852 (2019).
[54]D. Bayerl and E. Kioupakis, Appl. Phys. Lett. **115**, 131101 (2019).
[55]Q. Wen, Y. Wu, P. Wang, D. Laleyan, D. Bayerl, E. Kioupakis, Z. Mi, and M. Kira, Appl. Phys. Lett. **116**, 181103 (2020).
[56]A. Maity, S. J. Grenadier, J. Li, J. Y. Lin, and H. X. Jiang, Prog. Quantum Electron. **76**, 100302 (2021).
[57]H. Prevost, A. Andrieux-Ledier, N. Dorval, F. Fossard, J. S. Mérot, L. Schué, A. Plaud, E. Héripré, J. Barjon, and A. Loiseau, 2D Mater. **7**, 045018 (2020).
[58]C. R. Dean, A. F. Young, I. Meric, C. Lee, L. Wang, S. Sorgenfrei, K. Watanabe, T. Taniguchi, P. Kim, K. L. Shepard, and J. Hone, Nat. Nanotechnol. **5**, 722–726 (2010).

[59]J. Wu, J. Appl. Phys. **106**, 011101 (2009).
[60]N. Sanders, D. Bayerl, G. Shi, K. A. Mengle, and E. Kioupakis, Nano Lett. **17**, 7345–7349 (2017).
[61]J. Dong, L. Zhang, X. Dai, and F. Ding, Nat. Commun. **11**, 5862 (2020).
[62]V. Consonni, M. Knelangen, L. Geelhaar, A. Trampert, and H. Riechert, Phys. Rev. B **81**, 085310 (2010).
[63]S. M. Sadaf, S. Zhao, Y. Wu, Y. H. Ra, X. Liu, S. Vanka, and Z. Mi, Nano Lett. **17**, 1212–1218 (2017).
[64]Y. Wu, X. Liu, P. Wang, D. A. Laleyan, K. Sun, Y. Sun, C. Ahn, M. Kira, E. Kioupakis, and Z. Mi, Appl. Phys. Lett. **116**, 013101 (2020).
[65]V. Davydov, E. M. Roginskii, Y. Kitaev, A. Smirnov, I. Eliseyev, E. Zavarin, W. Lundin, D. Nechaev, V. Jmerik, M. Smirnov, M. Pristovsek, and T. Shubina, Nanomaterials **11**, 2396 (2021).
[66]C. Liu, Y. K. Ooi, S. M. Islam, H. Xing, D. Jena, and J. Zhang, Appl. Phys. Lett. **112**, 011101 (2018).
[67]L. Lymperakis, T. Schulz, C. Freysoldt, M. Anikeeva, Z. Chen, X. Zheng, B. Shen, C. Chèze, M. Siekacz, X. Q. Wang, M. Albrecht, and J. Neugebauer, Phys. Rev. Mater. **2**, 011601 (2018).
[68]Y. Wang, X. Rong, S. Ivanov, V. Jmerik, Z. Chen, H. Wang, T. Wang, P. Wang, P. Jin, Y. Chen, V. Kozlovsky, D. Sviridov, M. Zverev, E. Zhdanova, N. Gamov, V. Studenov, H. Miyake, H. Li, S. Guo, X. Yang, F. Xu, T. Yu, Z. Qin, W. Ge, B. Shen, and X. Wang, Adv. Opt. Mater. **7**, 1801763 (2019).
[69]X. Rong, X. Wang, S. V. Ivanov, X. Jiang, G. Chen, P. Wang, W. Wang, C. He, T. Wang, T. Schulz, M. Albrecht, V. N. Jmerik, A. A. Toropov, V. V. Ratnikov, V. I. Kozlovsky, V. P. Martovitsky, P. Jin, F. Xu, X. Yang, Z. Qin, W. Ge, J. Shi, and B. Shen, Adv. Mater. **28**, 7978–7983 (2016).
[70]V. Jmerik, D. Nechaev, K. Orekhova, N. Prasolov, V. Kozlovsky, D. Sviridov, M. Zverev, N. Gamov, L. Grieger, Y. Wang, T. Wang, X. Wang, and S. Ivanov, Nanomaterials **11**, 2553 (2021).
[71]S. M. Islam, K. Lee, J. Verma, V. Protasenko, S. Rouvimov, S. Bharadwaj, H. Xing, and D. Jena, Appl. Phys. Lett. **110**, 041108 (2017).
[72]J. Stachurski, S. Tamariz, G. Callsen, R. Butté, and N. Grandjean, Light Sci Appl. **11**(14), 114 (2022).
[73]Z. Y. Al Balushi, K. Wang, R. K. Ghosh, R. A. Vila, S. M. Eichfeld, J. D. Caldwell, X. Qin, Y. C. Lin, P. A. DeSario, G. Stone, S. Subramanian, D. F. Paul, R. M. Wallace, S. Datta, J. M. Redwing, and J. A. Robinson, Nat. Mater. **15**, 1166–1171 (2016).
[74]W. Wang, Y. Zheng, X. Li, Y. Li, H. Zhao, L. Huang, Z. Yang, X. Zhang, and G. Li, Adv. Mater. **31**, e1803448 (2019).
[75]B. Pecz, G. Nicotra, F. Giannazzo, R. Yakimova, A. Koos, and A. Kakanakova-Georgieva, Adv. Mater. **33**, e2006660 (2021).
[76]Y. Chen, K. Liu, J. Liu, T. Lv, B. Wei, T. Zhang, M. Zeng, Z. Wang, and L. Fu, J. Am. Chem. Soc. **140**, 16392–16395 (2018).
[77]N. Syed, A. Zavabeti, K. A. Messalea, E. Della Gaspera, A. Elbourne, A. Jannat, M. Mohiuddin, B. Y. Zhang, G. Zheng, L. Wang, S. P. Russo, E. Dorna, C. F. McConville, K. Kalantar-Zadeh, and T. Daeneke, J. Am. Chem. Soc. **141**, 104–108 (2019).
[78]P. Wang, T. Wang, H. Wang, X. Sun, P. Huang, B. Sheng, X. Rong, X. Zheng, Z. Chen, Y. Wang, D. Wang, H. Liu, F. Liu, L. Yang, D. Li, L. Chen, X. Yang, F. Xu, Z. Qin, J. Shi, T. Yu, W. Ge, B. Shen, and X. Wang, Adv. Funct. Mater. **29**, 1902608 (2019).
[79]E. Zdanowicz, A. P. Herman, K. Opołczyńska, S. Gorantla, W. Olszewski, J. Serafińczuk, D. Hommel, and R. Kudrawiec, ACS Appl. Mater. Interfaces **14**(4), 6131–6137 (2022).
[80]A. Pakdel, Y. Bando, and D. Golberg, Chem. Soc. Rev. **43**, 934–959 (2014).
[81]H. X. Jiang and J. Y. Lin, Patent No. 0268-1242 (2014).
[82]Y. Gao, W. Ren, T. Ma, Z. Liu, Y. Zhang, W.-B. Liu, L.-P. Ma, X. Ma, and H.-M. Cheng, ACS Nano **7**, 5199–5206 (2013).
[83]D. A. Laleyan, S. R. Zhao, S. Y. Woo, H. N. Tran, H. B. Le, T. Szkopek, H. Guo, G. A. Botton, and Z. T. Mi, Nano Lett. **17**, 3738–3743 (2017).
[84]P. Wang, W. Lee, J. P. Corbett, W. H. Koll, N. M. Vu, D. A. Laleyan, Q. Wen, Y. Wu, A. Pandey, J. Gim, D. Wang, D. Y. Qiu, R. Hovden, M. Kira, J. T. Heron, J. A. Gupta, E. Kioupakis, and Z. Mi, Adv. Mater. **34**, e2201387 (2022).
[85]K. A. Mengle and E. Kioupakis, APL Mater. **7**, 021106 (2019).
[86]X. Hai, R. T. Rashid, S. M. Sadaf, Z. Mi, and S. Zhao, Appl. Phys. Lett. **114**, 101104 (2019).
[87]X. Sun, P. Wang, T. Wang, L. Chen, Z. Chen, K. Gao, T. Aoki, M. Li, J. Zhang, T. Schulz, M. Albrecht, W. Ge, Y. Arakawa, B. Shen, M. Holmes, and X. Wang, Light: Sci. Appl. **9**, 159 (2020).
[88]G. Grosso, H. Moon, B. Lienhard, S. Ali, D. K. Efetov, M. M. Furchi, P. Jarillo-Herrero, M. J. Ford, I. Aharonovich, and D. Englund, Nat. Commun. **8**, 705 (2017).
[89]O. Schubert, M. Hohenleutner, F. Langer, B. Urbanek, C. Lange, U. Huttner, D. Golde, T. Meier, M. Kira, S. W. Koch, and R. Huber, Nat. Photonics **8**, 119–123 (2014).
[90]M. Kira, G. Roumpos, and S. T. Cundiff, Semicond. Semimetals **105**, 417–460 (2020).
[91]P. Wang, D. Wang, B. Wang, S. Mohanty, S. Diez, Y. Wu, Y. Sun, E. Ahmadi, and Z. Mi, Appl. Phys. Lett. **119**, 082101 (2021).
[92]D. Wang, P. Wang, B. Wang, and Z. Mi, Appl. Phys. Lett. **119**, 111902 (2021).